Optical response of stoichiometric and congruent lithium niobate from first-principles calculations

A. Riefer,* S. Sanna, A. Schindlmayr, and W. G. Schmidt
Department Physik, Universität Paderborn, 33095 Paderborn, Germany
(Received 4 March 2013; published 24 May 2013)

The frequency-dependent dielectric function and the second-order polarizability tensor of ferroelectric $LiNbO_3$ are calculated from first principles. The calculations are based on the electronic structure obtained from density-functional theory. The subsequent application of the GW approximation to account for quasiparticle effects and the solution of the Bethe-Salpeter equation for the stoichiometric material yield a dielectric function that slightly overestimates the absorption onset and the oscillator strength in comparison with experimental measurements. Calculations at the level of the independent-particle approximation indicate that these deficiencies are, at least, partially related to the neglect of intrinsic defects typical for the congruent material. The second-order polarizability calculated within the independent-particle approximation predicts strong nonlinear coefficients for photon energies above 1.5 eV. The comparison with measured data suggests that the inclusion of self-energy effects in the nonlinear optical response leads to a better agreement with experiments. The intrinsic defects of congruent samples reduce the optical nonlinearities, in particular, for the 21 and 31 tensor components, further improving the agreement between experiments and theory.

DOI: 10.1103/PhysRevB.87.195208 PACS number(s): 71.20.Ps, 77.84.Ek, 78.40.Ha

I. INTRODUCTION

The electro-optic, photorefractive, and nonlinear optical properties of ferroelectric lithium niobate[1,2] [$LiNbO_3$ (LN)] are exploited in a large number of devices, such as optical modulators, acousto-optic devices, optical switches for gigahertz frequencies, Pockels cells, optical parametric oscillators, or Q-switching devices. The vast majority of actual applications and measurements employ congruent crystals grown by the Czochralski method. In fact, LN crystals are, in general, not stoichiometric LN (SLN) but congruent LN (CLN), i.e., Li deficient. Many physical properties, such as the Curie temperature, depend strongly on the existence of point defects related to doping or the Li deficiency of the congruent material.[3] There are also indications that the optical properties of SLN and CLN differ notably.[4,5] However, all existing first-principles studies of the linear[6,7] and nonlinear[8,9] optical properties are restricted to stoichiometric LN.

Generally, the polarization $\mathbf{P}$ of a medium may be expressed as a power series of the incident field $\mathbf{E}(\omega)$ of frequency ω. In components, it is given by

$$\begin{aligned} P_\alpha(\omega) = &\sum_\beta \chi^{(1)}_{\alpha\beta}(-\omega,\omega)E_\beta(\omega) \\ &+ \sum_{\beta\gamma} \chi^{(2)}_{\alpha\beta\gamma}(-\omega,\omega_1,\omega_2)E_\beta(\omega_1)E_\gamma(\omega_2) \\ &+ \sum_{\beta\gamma\zeta} \chi^{(3)}_{\alpha\beta\gamma\zeta}(-\omega,\omega_1,\omega_2,\omega_3)E_\beta(\omega_1)E_\gamma(\omega_2)E_\zeta(\omega_3) \\ &+ \cdots, \end{aligned} \tag{1}$$

where $\chi^{(n)}(\omega)$ is the nth-order frequency-dependent susceptibility. $\chi^{(1)}(\omega)$ is the linear susceptibility related to the usual dielectric tensor through

$$\varepsilon_{\alpha\beta}(\omega) = \delta_{\alpha\beta} + 4\pi\,\chi^{(1)}_{\alpha\beta}(-\omega,\omega). \tag{2}$$

$\chi^{(2)}(\omega) := \chi^{(2)}(-2\omega,\omega,\omega)$ is relevant for the process of second-harmonic generation (SHG), where 2ω is the frequency of the field generated by the polarization of the medium and ω is the frequency of the incident field. The present paper aims at a better understanding of the influence of nonstoichiometry on the LN optical response. Calculations for the ordinary and extraordinary dielectric functions as well as for the energy dependence of the four nonvanishing components of the second-order polarizability tensor are presented.

This article is organized as follows. In Sec. II, we outline our computational approach. In particular, we describe the models representing the stoichiometric and the defect-rich congruent LN as well as the methods used to calculate the ground-state electronic structure and the optical response. In Sec. III, we then present results for the electronic band structure, the linear dielectric function, and the nonlinear second-order polarizability tensor, analyzing the influence of electronic correlation and of defects in congruent samples. Finally, in Sec. IV, we summarize the findings.

II. COMPUTATIONAL METHOD

CLN is strongly Li deficient and exhibits a [Li]/[Nb] ratio of 0.94. At first sight, it might seem as if this could be well described by a supercell with 80 atoms, from which one Li atom is removed, resulting in a [Li]/[Nb] ratio of 0.9375. Such a supercell is easily constructed by a $2 \times 2 \times 2$ repetition of the primitive cell, which contains two formula units of $LiNbO_3$. However, a realistic simulation of the congruent material requires more than the mere adjustment of the Li concentration.[10] Several experimental investigations[11,12] have excluded the presence of oxygen vacancies V_O, which are the hallmark of most oxides, but instead revealed the presence of a large amount of Nb_{Li}^{+4} antisite defects [Fig. 1(b)].[13] These might be charge compensated either by Nb vacancies [Fig. 1(d)] where four V_{Nb}^{-5} compensate for five Nb_{Li}^{+4} antisites in the so-called *Nb site vacancy model* or by Li vacancies [Fig. 1(c)] where four V_{Li}^{-} compensate for one Nb_{Li}^{+4} antisite within the *Li site vacancy model*. Nowadays, the Li site vacancy model, which we denote by CLN(Li) in the following, is widely accepted and is used for the interpretation of the LN material properties. According to this model, we simulate CLN by a charge-neutral supercell containing 360 atoms, which we

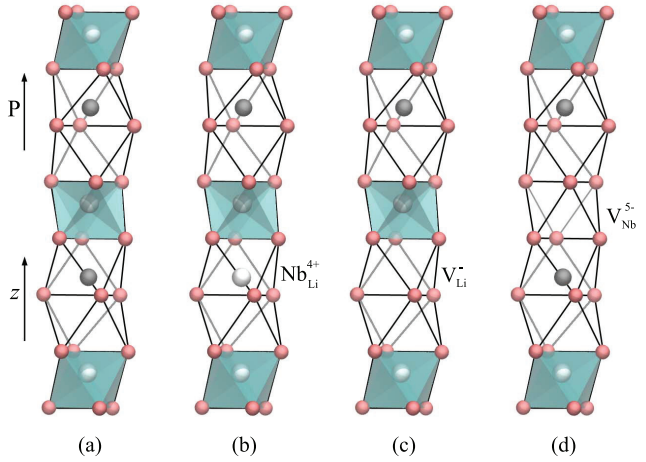

FIG. 1. (Color online) Schematic of (a) bulk SLN and the defects considered in the CLN models: (b) Nb_{Li}^{+4} antisite, (c) lithium vacancy V_{Li}^{-}, and (d) niobium vacancy V_{Nb}^{-5}. Oxygen atoms are red, Li atoms are black, and Nb atoms are white. The Nb octahedra are shaded, the z axis and the polarization direction are indicated.

construct by a $3 \times 3 \times 4$ repetition of the primitive cell, with one Nb_{Li}^{+4} antisite and four Li vacancies V_{Li}^{-}. This corresponds to a [Li]/[Nb] ratio of 0.92. For comparison, however, we also perform calculations within the Nb site vacancy model, denoted by CLN(Nb). In this case, a supercell of the same size containing five Nb_{Li}^{+4} antisites and four Nb vacancies V_{Nb}^{-5} is used, which again yields a [Li]/[Nb] ratio of 0.92.

The calculation of the optical response proceeds in three steps: First, we use density-functional theory (DFT) within the generalized gradient approximation (GGA) to obtain the structural and ground-state electronic properties of ferroelectric SLN and CLN. In detail, we employ the Vienna *ab initio* simulation package (VASP) implementation[14,15] of the projector-augmented-wave method. The wave functions are expanded into plane waves up to a cutoff energy of 400 eV, whereas, the mean-field effects of exchange and correlation are modeled with the PW91 functional.[16] A $6 \times 6 \times 6$ **k**-point mesh is used to sample the Brillouin zone corresponding to the primitive cell of bulk SLN. To determine the structural properties of CLN, including the relaxation of the atoms in the vicinity of the defect sites, with high accuracy, we choose $4 \times 4 \times 4$ **k**-points to sample the much smaller Brillouin zone corresponding to the 360-atom supercell. To compute the electronic and optical properties of CLN, we then change the sampling to $2 \times 2 \times 2$, which corresponds approximately to the same density of **k** points as the $6 \times 6 \times 6$ mesh used for SLN.

Second, the quasiparticle band structure is calculated within the GW approximation[17] (GWA) for the exchange-correlation self-energy. As usual, in practical applications of this scheme, we obtain the self-energy corrections to the electronic eigenvalue spectrum from a perturbative solution of the quasiparticle equation where the GGA exchange-correlation potential is replaced by the nonlocal and energy-dependent self-energy operator. We evaluate the latter in the standard non-self-consistent G_0W_0 approximation,[18] using the implementation described in Ref. 19, from the convolution of the single-particle propagator G_0 and the dynamically screened Coulomb interaction W_0 in the random-phase approximation.

Third, to obtain the linear dielectric function of SLN, we solve the Bethe-Salpeter equation (BSE) for coupled electron-hole excitations,[20–23] which incorporates the screened electron-hole attraction as well as the unscreened electron-hole exchange. Here, we use the time-evolution method described in Refs. 24 and 25 to obtain the polarizability.

Within the independent-particle approximation (IPA) or the independent-quasi-particle approximation (IQA), the linear dielectric function is given by

$$\varepsilon_{\alpha\beta}(\omega) = \delta_{\alpha\beta} + \frac{4\pi e^2}{\hbar m_e^2 V \omega^2} \sum_{n,m} \sum_{\mathbf{k}} f_{nm}(\mathbf{k}) \frac{p_{nm}^{\alpha}(\mathbf{k}) p_{mn}^{\beta}(\mathbf{k})}{\omega_{mn}(\mathbf{k}) - \tilde{\omega}}, \tag{3}$$

with the abbreviation $f_{nm}(\mathbf{k}) = f_{n\mathbf{k}} - f_{m\mathbf{k}}$, where $f_{n\mathbf{k}}$ and $f_{m\mathbf{k}}$ are the Fermi occupation factors for the Bloch states $|n\mathbf{k}\rangle$ and $|m\mathbf{k}\rangle$, respectively. Furthermore, V denotes the volume of the crystal, and $\tilde{\omega} = \omega + i\eta$ is the shorthand notation for the frequency ω with an additional small positive imaginary part η, which turns the electromagnetic field on adiabatically. The symbols,

$$p_{nm}^{\alpha}(\mathbf{k}) = \langle n\mathbf{k}|\hat{p}^{\alpha}|m\mathbf{k}\rangle \tag{4}$$

represent the momentum matrix elements of the system, and $\hbar\omega_{mn}(\mathbf{k}) = \epsilon_{m\mathbf{k}} - \epsilon_{n\mathbf{k}}$ are the transition energies between the bands m and n at the point **k**. The single-electron energies are taken from the DFT eigenvalue spectrum in the IPA and from the GWA quasiparticle band structure in the IQA.

Corresponding expressions for the coefficients of the second-order polarization tensor $\chi^{(2)}_{\alpha\beta\gamma}(\omega)$ were derived, e.g., in Refs. 26–28. Here, we postprocess the wave functions and eigenvalues from the VASP calculations and determine the nonlinear response as the sum of the two-band contribution,

$$\chi^{(2),\mathrm{two}}_{\alpha\beta\gamma}(\omega) = -\frac{ie^3}{m_e^3\hbar^2 V} \sum_{n,m} \sum_{\mathbf{k}} \frac{p_{nm}^{\alpha}(\mathbf{k})\{\Delta_{mn}^{\beta}(\mathbf{k}) p_{mn}^{\gamma}(\mathbf{k})\}}{[\omega_{mn}(\mathbf{k})]^4} \times f_{nm}(\mathbf{k}) \left(\frac{16}{\omega_{mn}(\mathbf{k}) - 2\tilde{\omega}} - \frac{1}{\omega_{mn}(\mathbf{k}) - \tilde{\omega}} \right), \tag{5}$$

and the three-band contribution,

$$\chi^{(2),\mathrm{three}}_{\alpha\beta\gamma}(\omega) = -\frac{ie^3}{m_e^3\hbar^2 V} \sum_{n,m,l}{}' \sum_{\mathbf{k}} \frac{p_{nm}^{\alpha}(\mathbf{k})\{p_{ml}^{\beta}(\mathbf{k}) p_{ln}^{\gamma}(\mathbf{k})\}}{\omega_{ln}(\mathbf{k}) - \omega_{ml}(\mathbf{k})} \times \left(\frac{16 f_{nm}(\mathbf{k})}{[\omega_{mn}(\mathbf{k})]^3[\omega_{mn}(\mathbf{k}) - 2\tilde{\omega}]} + \frac{f_{ml}(\mathbf{k})}{[\omega_{ml}(\mathbf{k})]^3[\omega_{ml}(\mathbf{k}) - \tilde{\omega}]} + \frac{f_{ln}(\mathbf{k})}{[\omega_{ln}(\mathbf{k})]^3[\omega_{ln}(\mathbf{k}) - \tilde{\omega}]} \right). \tag{6}$$

The prime for the sum symbol indicates that the summation only runs over index combinations $n \neq m \neq l$. As in the case of the linear dielectric function, the formulas can be evaluated either with independent-particle or independent-quasi-particle energies. To simplify the notation, we have defined

$$\{p_{ml}^{\beta}(\mathbf{k}) p_{ln}^{\gamma}(\mathbf{k})\} = \tfrac{1}{2}[p_{ml}^{\beta}(\mathbf{k}) p_{ln}^{\gamma}(\mathbf{k}) + p_{ml}^{\gamma}(\mathbf{k}) p_{ln}^{\beta}(\mathbf{k})]. \tag{7}$$

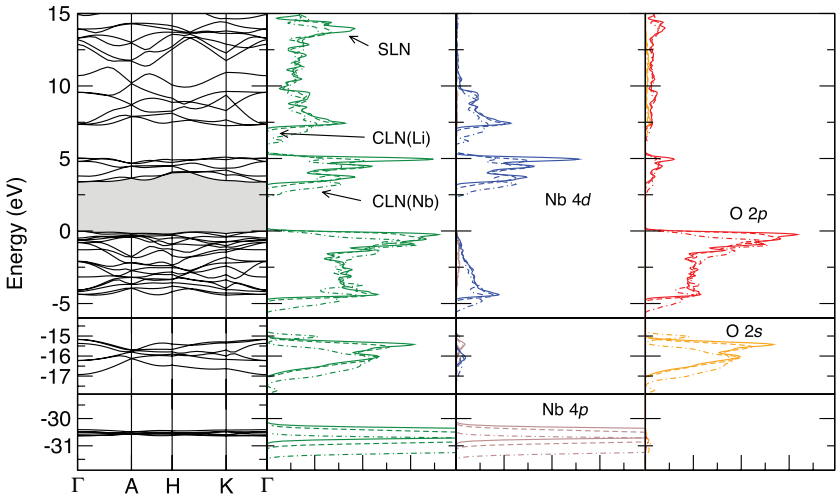

FIG. 2. (Color online) Electronic band structure of SLN within DFT-GGA together with the densities of states of SLN (solid line), CLN(Li) (dashed line), and CLN(Nb) (dashed-dotted line) in atomic units. The notation of the high-symmetry points follows Ref. 6. Separately shown are the O $2s$, O $2p$, Nb $4p$, and Nb $4d$ projected densities of states.

Finally, the matrix elements of the intraband transitions,

$$\Delta^{\beta}_{mn}(\mathbf{k}) = p^{\beta}_{mm}(\mathbf{k}) - p^{\beta}_{nn}(\mathbf{k}), \tag{8}$$

appearing in Eq. (5) are obtained from

$$p^{\beta}_{nn}(\mathbf{k}) = \frac{m_e}{\hbar}\partial_{k_\beta}\epsilon_n(\mathbf{k}). \tag{9}$$

Due to symmetry reasons, the second-order polarizability tensor of ferroelectric LN has four independent nonvanishing components $\chi^{(2)}_{\alpha\beta\gamma}(\omega)$, namely, the index combinations $211 = -222 = 112$, $223 = 131$, $311 = 322$, and 333. These are commonly labeled by the contracted indices $21 = -22 = 16$, $24 = 15$, $31 = 32$, and 33, respectively. These four components are studied in the present paper. We follow Ref. 29 concerning the notation for the Cartesian axes.

Calculated SHG data are known to be rather sensitive with respect to numerical details, such as the number of $\mathbf{k}$ points used to sample the Brillouin zone and the number of electronic bands included in the calculation.[30,31] Concerning the Brillouin-zone sampling, we find a $6 \times 6 \times 6$ $\mathbf{k}$-point mesh necessary to obtain converged spectra for SLN. The density of states (DOS) calculated at the DFT-GGA level is displayed in Fig. 2. It is characterized by a continuum of conduction bands and well-separated groups of valence bands. The latter are dominated by O $2p$ and Nb $4d$ states in the energy range between 0 and -5 eV by O $2s$ states between -15 and -17 eV and by Nb $4p$ states around -30.5 eV. These DOS features also determine the convergence of the SHG calculations. We find that the SHG spectra in the energy range up to 6 eV only vary weakly if the number of conduction bands increases above a cutoff energy of about 20 eV. The results are essentially converged for a cutoff energy of about 25 eV, which is, hence, used in the following. The dependence of the SHG data on the number of valence bands included in the calculation is more complex, however. Whereas, the inclusion of the O $2p$, Nb $4d$, and O $2s$ states already yields relatively well-converged 21 and 24 components of the second-order polarizability tensor, the 31 and 33 components exhibit an oscillatory behavior and require the additional inclusion of the Nb $4p$ states in the calculation. The transitions between the Nb $4p$ and the Nb $4d$ states cause noticeable modifications in the intensity of the three-band contribution (6) for these elements as illustrated below in Fig. 4. On the other hand, the inclusion of states below -36 eV has no impact on the calculated spectra for photon energies up to 6 eV.

III. RESULTS AND DISCUSSION

In Fig. 3, we show the calculated linear optical response of ferroelectric SLN according to the three levels of theory described in Sec. II, i.e., within (i) the IPA based on the DFT eigenstates and eigenenergies, (ii) within the IQA where the electronic self-energy is either obtained from the GWA or simply approximated by a scissors operator that widens the fundamental gap by 2.03 eV, and (iii) from the solution of the BSE. The spectra obtained within the IPA show two main features of the optical absorption around 5 and 8 eV. The inclusion of self-energy effects within the GWA leads to a nearly rigid blueshift in the spectra by about 2 eV. The GWA spectra shown here differ slightly from our previous results[6] where the self-energy was evaluated with a model dielectric function rather than the fully frequency-dependent random-phase approximation employed here. We find that the self-energy effects in the present calculations can be simulated very well by a simple Sci shift of 2.03 eV as illustrated in Fig. 3. The inclusion of the Coulomb correlation between electrons and holes by means of the BSE both repositions the spectrum on the energy axis and changes the line shapes. The first peak of the low-energy main feature of the optical absorption becomes more pronounced, and the entire structure is redshifted relative to the GWA. It is now centered at 5.5 and 5.6 eV for $\varepsilon_\perp$ or $\varepsilon_\parallel$, respectively. The oscillator strength of the originally rather broad ($\sim$2 eV) high-energy main feature of the optical absorption is also redshifted and transferred into a single sharp peak at about 9.3 eV for $\varepsilon_\perp$ and $\varepsilon_\parallel$. This peak originates mainly from electronic transitions that involve the O $2p$ valence states and conduction states with energies of between 6 and 8 eV.

The comparison of the BSE calculations for SLN with experimental data[32,33] shows qualitative agreement but clear deviations concerning some quantitative details. On one hand, the calculations overestimate the onset of the optical absorption by about 0.2 eV. On the other hand, the double-peak structure of the first absorption maximum is far more

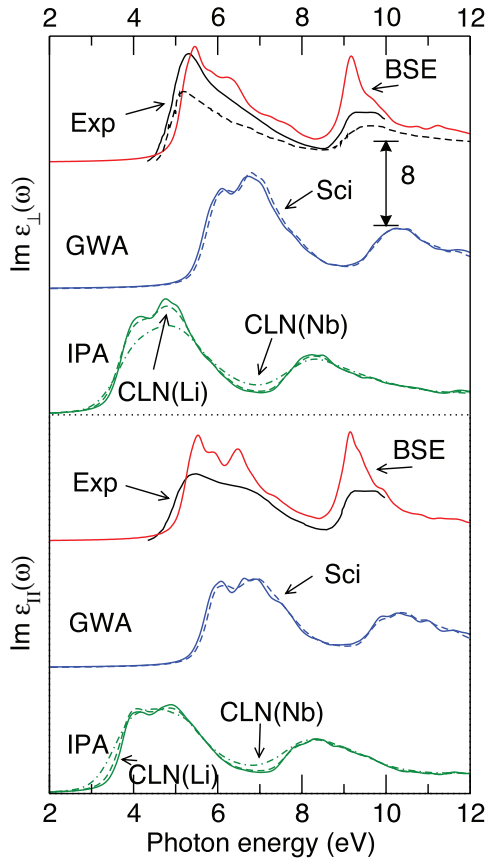

FIG. 3. (Color online) Imaginary part of the ordinary (above) and extraordinary (below) dielectric function of ferroelectric SLN. In both cases, we compare the IPA with results that include quasiparticle self-energy effects either evaluated within the GWA or obtained from a scissors (Sci) operator, as well as the solution of the Bethe-Salpeter equation (BSE), which includes electron-hole attraction and local-field effects. Also shown are IPA calculations for CLN together with experimental data (solid line: Ref. 32, dashed line: Ref. 33).

pronounced in the calculations than observed experimentally. This may partially be related to temperature effects, which are neglected in the present calculations. Furthermore, deviations between experiments and our calculations can be expected due to the modified stoichiometry and structure of congruent LN compared to the stoichiometric material considered so far. In order to explore the differences between the optical response of CLN and SLN, we now turn to the former, using the CLN(Li) and CLN(Nb) models introduced in Sec. I. Since realistic simulations require large supercells with 360 atoms, these calculations are restricted to the IPA level of theory. As can be seen in Fig. 3, the differences in the linear optical response between the CLN(Li) model and the SLN are rather small. Slightly more pronounced are the changes that arise if the CLN(Nb) structure for the congruent material is used. Irrespective of the model underlying the calculations, however, we observe the same trend: The onset of optical absorption is redshifted by up to 0.2 eV for CLN in comparison to SLN, especially for $\varepsilon_{\parallel}$, and the double-peak structure of the first absorption maximum is washed out, most notably for $\varepsilon_{\perp}$. As a consequence, the results for CLN are closer to the experimental data for the linear optical response than the SLN calculations. However, it should be kept in mind that the differences in the optical response between CLN and SLN, which we have studied here in the IPA, may be affected by many-body effects and show a different behavior at the level of the BSE. In particular, large exciton binding energies for localized defect states (see, e.g., Ref. 34) may further increase the optical-absorption redshift in CLN compared to stoichiometric samples.

In order to understand the smoothing of the double-peak feature for $\varepsilon_{\perp}$ in the range between 3.5 and 5.5 eV due the defects typical for CLN, we analyzed the joint density of states (JDOS) as well as the oscillator strengths of the relevant transitions. We find the JDOS to be very similar for SLN and CLN, apart from a reduction in the gap in the congruent material, which can already be identified in the DOS displayed in Fig. 2, and a rather uniform intensity reduction for energy differences above 4.5 eV. The fine structure of the first absorption maximum is found to be caused by the oscillator strengths rather than the JDOS, however. The fading of this fine structure for CLN is mainly related to the reduced transition matrix elements between the O $2p$ valence states and the Nb $4d$ conduction states. The redshift in the absorption onset, on the other hand, is caused by the modified DOS.

In Fig. 4, we present the 21, 24, 31, and 33 components of the second-order polarizability tensor for ferroelectric LN calculated within the IPA. Both the real and the imaginary parts of $\chi^{(2)}(\omega)$ are shown up to 6 eV. The main features of the SHG spectra lie between 1.5 and 3.0 eV with additional strong nonlinearities at higher energies in the range between 4 and 5 eV, in particular, for the 21 and 31 components. The present results for the 33 component are very similar to earlier IPA calculations[9] that neglected intraband transitions and considered only the three-band contribution (6). We find that the inclusion of the two-band term (5) only leads to marginal changes in the case of LN and neither affects the line shapes nor the magnitude of the SHG coefficients substantially. The differences between the present calculations and the paper by Cabuk[45] appear more pronounced, on the other hand, but these are partially related to the different broadening parameters η. In fact, if we decrease the broadening from 0.15 eV, the value used in our calculations, to 0.05 eV, then the obtained line shapes are in good correspondence with those in Ref. 45. In particular, the 33 component shows a very similar spectral dependence.

The SHG coefficients are strongly affected by self-energy effects. As demonstrated above in connection with Fig. 3, the energy and **k** dependence of the quasiparticle corrections are sufficiently small to allow for their approximation by a scissors operator. Therefore, here, we follow the same approach to obtain the second-order polarizability at the IQA level of theory. The results are displayed in Fig. 4. We observe a blueshift in the SHG features by about 1 eV if self-energy effects are included, accompanied by a notable lowering of the intensity. The dependence of the SHG spectra on transitions involving the Nb $4p$ states is also illustrated in Fig. 4. Evidently, the inclusion of the Nb $4p$ states does not give rise to any new spectral signatures in the energy range considered here, but it modifies the intensities considerably, in particular, for the 31 and 33 components.

Several experimental measurements of SHG data for LN have been reported in the literature.[35–44] The available data

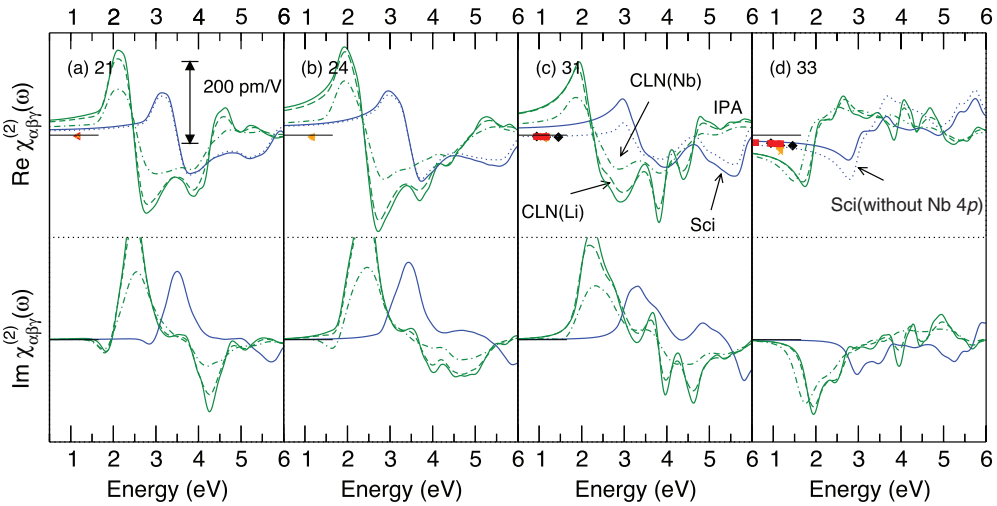

FIG. 4. (Color online) Coefficients of the second-order polarizability tensor $\chi^{(2)}(\omega)$ for SLN and CLN calculated within the IPA and with a Sci shift, compared to experimental data from Refs. 35–43 (diamonds, squares, crosses, plusses, left triangles, right triangles, down triangles, up triangles, and stars). We follow the notation of Ref. 44 concerning the orientation of the axes and apply the scaling described in Ref. 35. Sci(without Nb $4p$) denotes calculations that do not include the Nb $4p$ states.

points are indicated by symbols in Fig. 4. We also include measurements of the modulus $|\chi^{(2)}(\omega)|$ and take these to represent the real part of the polarizability because the imaginary part is very small in the energy region experimentally probed. The comparison with the calculated spectra at the IPA and IQA levels of theory in Fig. 4 shows that the former clearly overestimates the measured data, whereas, the IQA calculations, which include electronic self-energy effects, describe the optical nonlinearities better, especially the 33 component. Nevertheless, even the IQA calculations for SLN still yield stronger nonlinearities than observed experimentally. In this respect, it is interesting to note that the CLN results at the IPA level of theory indicate that the congruent material gives rise to weaker SHG signals than predicted for SLN. This holds, in particular, for CLN(Nb). In addition, for the Nb site vacancy model, the spectra are somewhat smoothed, and the features are redshifted. In the case of the 33 component, this leads to an enhanced signal in the energy region experimentally probed. As for the linear response, the proper inclusion of defects in the congruent material, thus, also seems to improve the agreement between experiments and theory concerning $\chi^{(2)}(\omega)$.

A word of caution is necessary when comparing the experimental and theoretical data, however. First, all of the experimental values are clearly in the nonresonant region around 1 eV and, in particular, for the 21, 24, and 31 components, of very low absolute magnitude. We remark that the intensity is, e.g., 2 orders of magnitude lower than the SHG signal of GaAs in this region. Second, the effects of the crystal local fields and the electron-hole interaction are not included in the present SHG calculations. Luppi *et al.*,[46] for instance, found that $\chi^{(2)}(\omega)$ can decrease up to 30% due to local-field effects, depending on the material and on the frequency range. Excitonic effects, on the other hand, are expected to lead to a rather uniform but noticeable increase in the SHG signal.[28,46]

IV. SUMMARY

Our paper represents an attempt towards a first-principles description of the optical response of congruent lithium niobate. The linear and nonlinear optical responses calculated for the Li site vacancy model as well as the Nb site vacancy model are shown to be closer to the available experimental data than the spectra calculated for stoichiometric crystals: Compared to SLN, the CLN simulations lead to a redshift in the spectral features, wash out part of the fine structure, and reduce the nonlinearities. This holds, in particular, for CLN(Nb). It is clear, however, that further work is required to fully understand the influence of crystal imperfections on the optical response of lithium niobate. On one hand, a variety of further defect configurations and defect complexes will have to be investigated, see, e.g., Ref. 47. In this respect, the structure models adopted in this paper are created by placing the defects at randomly chosen lattice sites and can be further refined by taking clustering phenomena into account.[48] On the other hand, we expect many-body effects, which here, were shown to have a strong impact on the optical response of SLN, to give rise to even stronger modifications of the CLN signal.

ACKNOWLEDGMENTS

We gratefully acknowledge financial support from the DFG as well as supercomputer time provided by the HLRS Stuttgart and the Paderborn PC^2.

*riefer@mail.upb.de

[1] A. Räuber, Curr. Top. Mater. Sci. **1**, 481 (1978).
[2] R. S. Weis and T. K. Gaylord, Appl. Phys. A **37**, 191 (1985).
[3] L. Galambos, S. S. Orlov, L. Hesselink, Y. Furukawa, K. Kitamura, and S. Takekawa, J. Cryst. Growth **229**, 228 (2001).

[4]I. V. Kityk, M. Makowska-Janusik, M. D. Fontana, M. Aillerie, and F. Abdi, J. Appl. Phys. **90**, 5542 (2001).
[5]I. V. Kityk, M. Makowkska-Janusik, M. D. Fontana, M. Aillerie, and F. Abdi, J. Phys. Chem. B **105**, 12242 (2001).
[6]W. G. Schmidt, M. Albrecht, S. Wippermann, S. Blankenburg, E. Rauls, F. Fuchs, C. Rödl, J. Furthmüller, and A. Hermann, Phys. Rev. B **77**, 035106 (2008).
[7]W. Y. Ching, Z.-Q. Gu, and Y.-N. Xu, Phys. Rev. B **50**, 1992 (1994).
[8]H. Akkus, S. Cabuk, and A. M. Mamedov, Int. J. Nanoelectron. Mater. **3**, 53 (2010).
[9]A. Riefer, S. Sanna, A. V. Gavrilenko, and W. G. Schmidt, IEEE Trans. Ultrason. Ferroelectr. Freq. Control **59**, 1929 (2012).
[10]T. Volk and M. Wöhlecke, *Lithium Niobate: Defects, Photorefraction and Ferroelectric Switching*, Springer Series in Materials Science (Springer, Berlin, 2008), softcover reprint of hardcover, 1st ed. 2009.
[11]N. Zotov, H. Boysen, F. Frey, T. Metzger, and E. Born, J. Phys. Chem. Solids **55**, 145 (1994).
[12]A. P. Wilkinson, A. K. Cheetham, and R. H. Jarman, J. Appl. Phys. **74**, 3080 (1993).
[13]N. Iyi, K. Kitamura, F. Izumi, J. Yamamoto, T. Hayashi, H. Asano, and S. Kimura, J. Solid State Chem. **101**, 340 (1992).
[14]G. Kresse and J. Furthmüller, Comput. Mater. Sci. **6**, 15 (1996).
[15]G. Kresse and D. Joubert, Phys. Rev. B **59**, 1758 (1999).
[16]J. P. Perdew, J. A. Chevary, S. H. Vosko, K. A. Jackson, M. R. Pederson, D. J. Singh, and C. Fiolhais, Phys. Rev. B **46**, 6671 (1992).
[17]L. Hedin, Phys. Rev. **139**, A769 (1965).
[18]M. S. Hybertsen and S. G. Louie, Phys. Rev. B **34**, 5390 (1986).
[19]M. Shishkin and G. Kresse, Phys. Rev. B **74**, 035101 (2006).
[20]S. Albrecht, L. Reining, R. DelSole, and G. Onida, Phys. Rev. Lett. **80**, 4510 (1998).
[21]L. X. Benedict, E. L. Shirley, and R. B. Bohn, Phys. Rev. Lett. **80**, 4514 (1998).
[22]M. Rohlfing and S. G. Louie, Phys. Rev. Lett. **83**, 856 (1999).
[23]M. Palummo, O. Pulci, A. Marini, L. Reining, and R. DelSole, Phys. Rev. B **74**, 235431 (2006).
[24]W. G. Schmidt, S. Glutsch, P. H. Hahn, and F. Bechstedt, Phys. Rev. B **67**, 085307 (2003).
[25]P. H. Hahn, W. G. Schmidt, and F. Bechstedt, Phys. Rev. Lett. **88**, 016402 (2001).
[26]D. E. Aspnes, Phys. Rev. B **6**, 4648 (1972).
[27]J. L. P. Hughes and J. E. Sipe, Phys. Rev. B **53**, 10751 (1996).
[28]R. Leitsmann, W. G. Schmidt, P. H. Hahn, and F. Bechstedt, Phys. Rev. B **71**, 195209 (2005).
[29]S. Sanna and W. G. Schmidt, Phys. Rev. B **81**, 214116 (2010).
[30]M.-Z. Huang and W. Y. Ching, Phys. Rev. B **47**, 9464 (1993).
[31]R. E. Alonso, S. Sharma, C. Ambrosch-Draxl, C. O. Rodriguez, and N. E. Christensen, Phys. Rev. B **73**, 064101 (2006).
[32]E. Wiesendanger and G. Güntherodt, Solid State Commun. **14**, 303 (1974).
[33]A. M. Mamedov, M. A. Osman, and L. C. Hajieva, Appl. Phys. A: Solids Surf. **34**, 189 (1984).
[34]P. Rinke, A. Schleife, E. Kioupakis, A. Janotti, C. Rödl, F. Bechstedt, M. Scheffler, and C. G. Van de Walle, Phys. Rev. Lett **108**, 126404 (2012).
[35]I. Shoji, T. Kondo, A. Kitamoto, M. Shirane, and R. Ito, J. Opt. Soc. Am. B **14**, 2268 (1997).
[36]M. M. Choy and R. L. Byer, Phys. Rev. B **14**, 1693 (1976).
[37]G. D. Boyd, R. C. Miller, K. Nassau, W. L. Bond, and A. Savage, Appl. Phys. Lett. **5**, 234 (1964).
[38]D. A. Kleinman and R. C. Miller, Phys. Rev. **148**, 302 (1966).
[39]R. C. Miller and A. Savage, Appl. Phys. Lett. **9**, 169 (1966).
[40]J. Bjorkholm, IEEE J. Quantum Electron. **4**, 970 (1968).
[41]W. F. Hagen and P. C. Magnante, J. Appl. Phys. **40**, 219 (1969).
[42]R. C. Miller, W. A. Nordland, and P. M. Bridenbaugh, J. Appl. Phys. **42**, 4145 (1971).
[43]B. F. Levine and C. G. Bethea, Appl. Phys. Lett. **20**, 272 (1972).
[44]D. Roberts, IEEE J. Quantum Electron. **28**, 2057 (1992).
[45]S. Cabuk, Cent. Eur. J. Phys. **10**, 239 (2012).
[46]E. Luppi, H. Hübener, and V. Véniard, J. Chem. Phys. **132**, 241104 (2010).
[47]H. H. Nahm and C. H. Park, Phys. Rev. B **78**, 184108 (2008).
[48]H. Xu, D. Lee, J. He, S. B. Sinnott, V. Gopalan, V. Dierolf, and S. R. Phillpot, Phys. Rev. B **78**, 174103 (2008).